Simultaneous Track and Multi-Spectral Instrument for Satellite Identification

James Mason
Lockheed Martin
Jacob Wirth, Matthew Bold
Lockheed Martin

ABSTRACT

Current electro-optical sensors used for Space Domain Awareness (SDA) predominantly provide two types of data: angles data for orbit determination, and light curve data for characterization. While the light curve data has been very useful in establishing patterns of life and stability, there is more information which can be extracted from the available electro-optical signature. The utility of such higher degree of characterization includes a more detailed understanding of signature, change detection, as well as positive ID to resolve cross-tagging or re-establishing custody after track loss.

Prior studies into the utility of spectral data for characterization have demonstrated one of the fundamental issues of collecting spectral data – satellite optical signatures are often "photon-starved", and the act of spreading the solar photons reflected from the satellite into many spectral bins simply exacerbates the problem, reducing the signal to noise substantially.

Electro-optical sensors for SDA have shown their value when proliferated geographically at relatively low cost. While the signal to noise problem can be addressed by larger apertures, this diminishes the value of such sensors by driving cost higher. To recover signal to noise with affordable apertures, it becomes necessary to reduce the spectral resolution. This of course reduces the ability to resolve any fine spectral features.

We have incorporated a low-resolution spectrograph into one of the satellite tracking systems operated by the Lockheed Martin's Advanced Technology Center (ATC). The goal is to investigate the utility of lower resolution spectra for the purposes of positive ID and change detection. The spectrograph is constructed using a transmission grating at the exit pupil of the telescope optical system, right before the final imaging lens. This has the added value that the resulting imagery contains not only the spectra of the satellite from the 1st order diffraction of the grating, but metric track data as well by using the 0th order spot that passes through the grating.

The image processing and calibration is critical to retrieving useful spectra and must undergo a slightly different process than when processing ordinary track data for astro- and photometrics. The effect of a transmission grating is to generate both the 0^{th} order image as well as the shifted, spectrally dispersed 1^{st} order spectral image of the 0^{th} order image summed in the same array. Because it contains both images, normal flat fielding to correct for vignetting/non-uniformity would incorrectly re-scale the spectra. Instead, the flat field image needs to be fit to the background data and subtracted to preserve the spectral data.

Since the satellite is sun-illuminated, we calibrate the spectra by observing sun-like (G2V) stars at varying elevations, then interpolating between these reference spectra to the elevations of the satellite observations. This fit will account, to some extent, for spectral extinction of the atmosphere – dividing the processed satellite spectra by the sun-like reference spectra results in a reasonable estimation of the actual satellite color.

Results are presented of a small number of disparate and similar classes of LEO satellites, and the ability to provide discrimination between disparate classes, as well as the ability to classify similar classes of satellites using spectra is assessed.

1. INTRODUCTION

Situational awareness in the space domain is challenging. The distances are large and the objects are small, which makes it a challenge to sense these objects. These objects can be imaged, to understand what they are and what they are doing, but the sensors required to do so are very expensive, e.g. very large telescopes with adaptive optics or very powerful radars. In order to maintain custody of objects in the large volume of space, it is desirable to be able to proliferate geographically a large number of affordable sensors. These types of sensors, at least those that are optical, tend to only provide metric track and brightness data. Characterization then is limited to interpreting and

assessing changes to the light curve alone. While this provides some discrimination ability, there is more information which can be extracted from the sensed light.

There are two other phenomenologies which can be used to further exploit the optical signature. Polarization has been used to discriminate between satellites in geostationary earth orbit (GEO) [1]. Satellite spectra has an even greater promise to provide the ability to fingerprint satellites by exploiting the larger number of degrees of freedom the spectrum offers. Previous methods have investigated this for both identification and the attempt to characterize material properties of satellites [2][3][4]. However, measuring spectra comes at the expense of decreased signal to noise – the more the photons are spread out, the harder it is to make the necessary measurements.

In 2023, an independent research and development (IRAD) program began to investigate the utility of using a transmission grating in order to generate both track data (the 0th order, un-diffracted light) as well as spectral data (1st order diffracted light) on the same focal plane [5], focusing on investigating the utility of a relatively low resolution spectrograph to aid in satellite characterization and change detection. The choice of using a low-resolution spectrograph is to minimize to some extent the loss of signal to noise in the spectra, with the understanding that the optimal resolution is still to be determined.

For the purposes of experimentation, discrimination, and testing, the Chinese Yaogan constellation provides a convenient testing ground [6]. Approximately 120 satellites make up this low earth orbit (LEO) constellation, spanning different mission functions from electro optical (EO) to electronic intelligence (ELINT) and synthetic aperture radar (SAR). The plan is to track as many of these as possible and attempt to discern the differences and similarities between the various mission applications and/or manufacturers. A stretch goal would be to be able to apply what's learned from the various documented Yaogan series to those Yaogan satellites for which the function has not been publicly stated.

2. INSTRUMENT DESCRIPTION

Lockheed Martin's ATC team has developed several optical sensors for tracking and characterization of satellites, such as the Space Object Tracking observatory in the Santa Cruz Mountains [7]. Another system is the Satellite Tracking and Illumination LADAR Trailer (STILT). STILT utilizes a 0.5 meter Coudé telescope mounted on a 5'x12' optical bench in a mobile 40' trailer, shown in Fig. 1. The telescope is a 10:1 afocal Mersenne, followed by two dichroic lenses which generate a 30 mm exit pupil in front of the imaging sensor. The visible imaging sensor is a 50 mm Nikon lens with an Andor NEO 5.5 sCMOS camera. The STILT system has been often used for laser tracking of satellites in the past, with an 8" VIS/NIR dichroic placed close to M7 (prior to the pupil imaging lens pair), but in general it is also a very useful optical system for prototyping novel optical sensors for space domain awareness (SDA), given the Coudé design which brings the light to a large optical bench.

Figure 1: *The Satellite Tracking and Illumination LADAR Trailer, showing the roll-back roof and the 0.5 meter Coudé path telescope. The telescope sits on a 5'x12' optical bench inside the trailer.*

In this case, the modifications of the sensor are quite simple due to the space available on the optical bench, and the presence of an exit pupil in front of the imaging lens of the camera. A commercial off the shelf (COTS) transmission grating (Richardson 751-R, 75 grooves per mm, nominal blaze wavelength 730 nm) is placed at the exit pupil. A Zemax model is shown in Fig. 2. The grating generates the 0th order spot as well as the 1st (and higher) diffraction

order streaks which contain the spectral information. The combination of the grating, the imaging lens, and a 2x2 binning in the Andor camera results in a R between 130 and 260 in the expected spectral band (0.45 to 0.9 um).

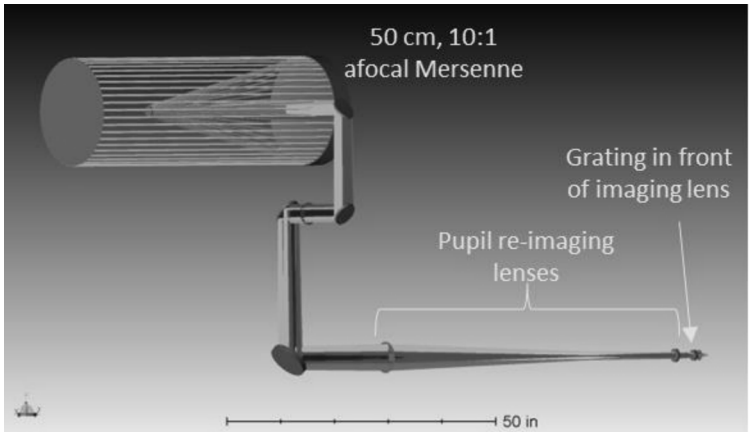

Figure 2: *Zemax model of the 0.5 meter system, including the two lenses to reimage the input pupil at the camera. The optical components are all COTS, thus the rather large footprint. The transmission grating is placed at the exit pupil, in front of the final imaging lens.*

3. IMAGE PROCESSING AND CALIBRATION

It is important to note that the goal of this initial investigation is to measure enough spectral signatures of satellites to determine whether this type of sensor can provide sufficient information to allow for object discrimination and identification. Thus the goal is explore the phenomenology of the *shape* of the spectral signatures from various satellites, and not (yet) to generate calibrated magnitudes.

3.1 Grating Calibration

The first step in calibration is to derive the mapping between pixel location, relative to the 0th order track point centroid, and wavelength. This is done using a Kr light source as shown in Fig 3

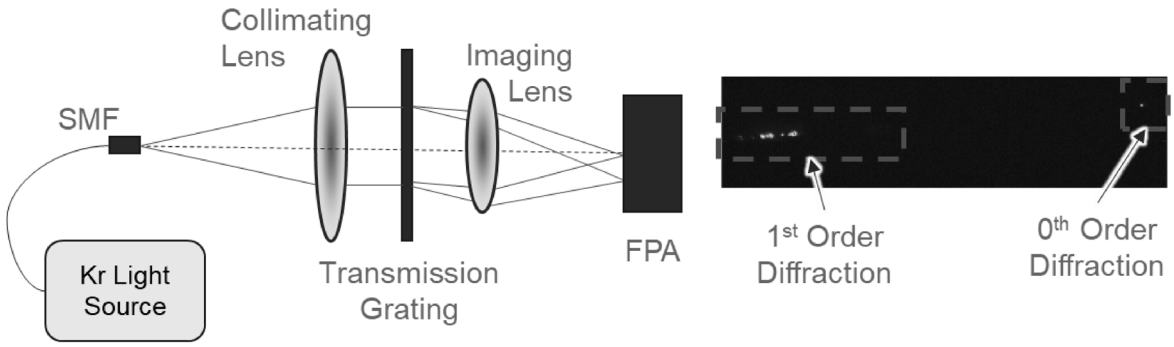

Figure 3: *On the left, the schematic layout of the grating calibration setup. The fiber coupled Kr light source is collimated, put through the grating, and imaged onto the camera. An image of the diffracted calibration light is shown on the right with the 0th and 1st order diffraction patterns highlighted.*

The measured peaks are then compared to NIST calibration data [8]. This is shown in Fig 4.

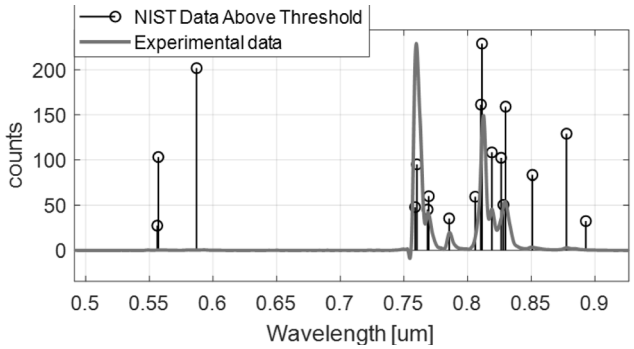

Figure 4: *Mapping of Kr lines to measured peaks is done manually, then the data is fit using a 3rd order polynomial.*

As can be seen, only 6 of the lines in the 750-850 nm range were identified, which may cause some skew to the calibration. A third order polynomial was used to map pixels to wavelength with very good results.

Table 1: *Third order polynomial constants used to map pixel location to wavelength spectra.*

Polynomical coefficient	Value
P_0	-0.256
P_1	7.15e-3
P_2	-1.83e-5
P_3	2.89e-8

3.2 Background Estimation

Removal of the background counts in the image is critical to accurately estimating the magnitude of satellite reflected light in each of the spectral pixel bins. The software tool SExtractor [9] for astronomical image processing was used to do the background estimation. Tests on data demonstrated very successful estimation with no appreciable bias remaining in the image. An example is shown in Fig. 5

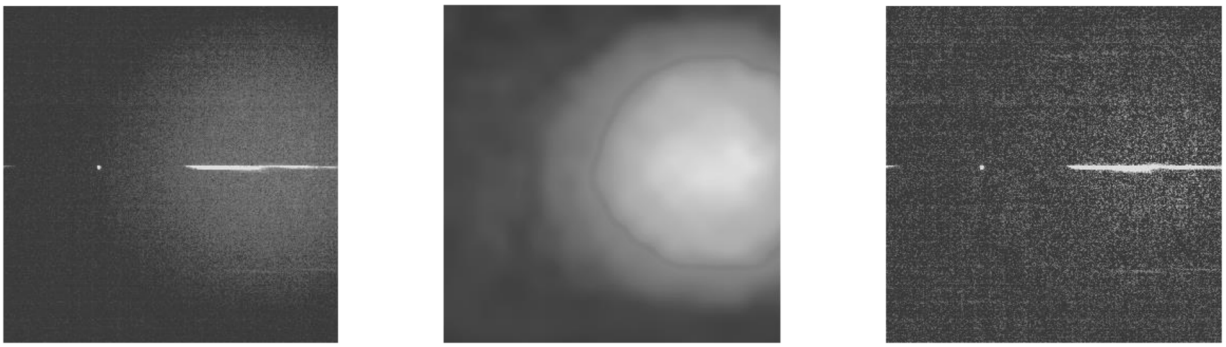

Figure 5: *Images showing the background subtraction process. On the left, a raw image from the camera, uncorrected. The round glow on the right is actually the 1st order diffracted sky, as the optical system, without the grating, is fairly well centered in the image. Also visible is the start of the -1st order on the left side, as well as the +2nd order on the far right of the image. In the middle is the background estimation map, using an algorithm which does sigma clipped median estimations on subarrays of the left image, then does a bicubic spline interpolation to create the background map. On the right is the background subtracted image, showing good bias subtraction. Cumulative sums were performed column-wise to ensure no systematic bias was left.*

3.3 Spectra Processing

Once the background has been subtracted, the SExtractor software tool is used to estimate the centroid of the 0th order blob. This centroid value is then used as the (0,0) point from which to box the spectral data as shown in Fig. 6. Counts are then summed along the columns to estimate the total flux in each spectral bin. No attempt has been made yet to optimize the width of the box to minimize the noise contribution to the sum. The box length was chosen just short of one octave, to ensure that no contribution from the 2nd order spectra contaminates the measurement.

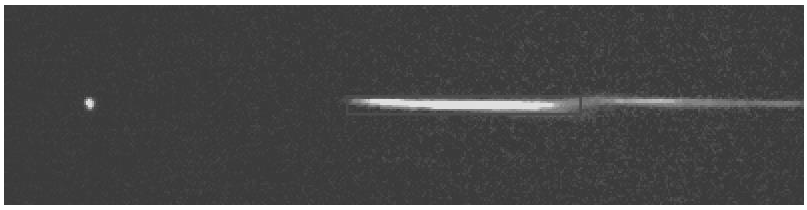

Figure 6: *Zoom in on the processed spectral data. The 0th order spot is on the left, the red box is the extracted spectra, from approximately 0.43 to 0.82 um. The red boxed subarray is summed column-wise to get spectral counts per pixel bin. Further to the right, the 2nd order diffraction streak is seen.*

A second output of the SExtractor processing is to estimate the number of counts in the 0th order blob. The summed spectral data is divided by the 0th order flux so as to normalize the spectra and remove the effects of changing overall intensity. As noted earlier, this particular investigation is focusing on looking at the characteristic and shape of the spectra, as well as how that shape changes, thus normalizing to the satellite brightness is the approach taken.

3.4 Spectral Calibration

The measured satellite spectra from the solar reflected light can be expressed as

$$DN_\lambda = E_\lambda \cdot R_\lambda \cdot Atm_\lambda \cdot Sensor_\lambda$$

Where DN_λ are the digital counts output by the camera, E_λ is the spectral irradiance of the Sun, R_λ is the reflectivity of the satellite, Atm_λ is the atmospheric transmission, and $Sensor_\lambda$ is a combination of the optical transmission, grating efficiency and camera responsivity and gain. Of these four terms, R_λ is the desired quantity to be estimated, the rest of the terms need to be calibrated out of the measurement. This is most easily done by taking spectra of a Sun-like star using the same instrument on the same night, and preferably at the same location in the sky as the satellite. In general this last desirement is hard to achieve, so taking measurements of several Sun-like stars over a range of elevations can be used to determine the spectral atmospheric extinction at the elevation of the satellite. Of course, if the weather is not particularly good (e.g. high cirrus or other effects), this approach may not be very accurate.

The Sun-like characterization is most easily achieved by picking stars of the same temperature, for which the B-V color index is used. The Sun is a G2V star (5,770 K) with color index 0.65. The Tycho 2 catalog was used, filtering on the B-V color index between 0.64 and 0.655, which closely brackets the G2V color without encroaching on the G1V (5,860 K) or the G3V (5,720 K) category stars.

Fig. 7 shows the measured spectra from three G2V stars taken on 7 August 2023, at three different elevations. While the agreement between the three spectra is quite good, it is puzzling that a greater discrepancy is not seen at the short wavelength end of the spectra, as the elevations vary from 25 to 70 degrees. Often, the two main components of atmospheric extinction, Rayleigh and aerosol scatter are somewhat similar in magnitude, thus the Rayleigh term, with its λ^{-4} wavelength dependence is obvious. However, in this case, it is speculated that the aerosol term, which is wavelength independent, may be dominating, making the Rayleigh contribution difficult to see.

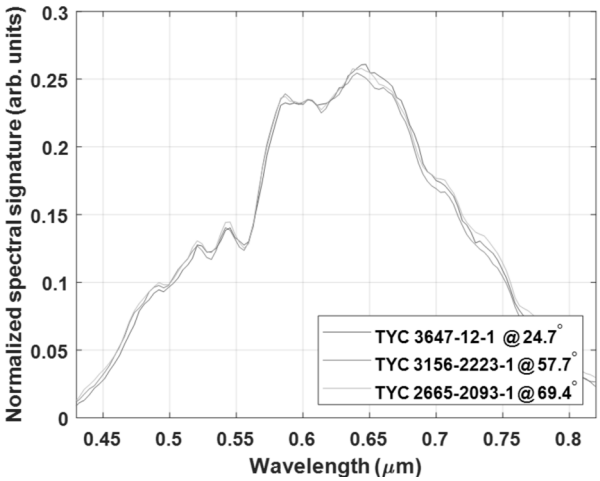

Figure 7: *Spectra of three G2V stars (Tycho 2 catalog identifiers in the plot legend) taken the night of the satellite tracking. It is acknowledged that it is puzzling that a stronger Rayleigh scatter signature is not seen at the shorter wavelengths, for the lower elevations.*

4. EXPERIMENTATION AND RESULTS

The integration of the instrument and its controls was completed in late July 2023, overcoming several technical issues, and one good night of satellite tracking was performed on 7 August (8 August UTC) prior to the writing of this paper. Four Yaogan satellites were tracked, listed in Table 2. One satellite's track, Yaogan 16a, was noisy enough that it wasn't used. Two contractors built these four satellites, the Chinese Academy of Space Technology (CAST) and the Shanghai Academy of Spaceflight Technology (SAST).

Table 2: *The list of the satellites tracked on the evening of 7 August, 2023. Yaogan 16a, however had excessive jitter in its track and the data was not usable.*

Name	SSN	Function	Contractor	Track duration
~~**Yaogan 16a**~~	~~39011~~	~~ELINT~~	~~CAST~~	~~186 sec~~
Yaogan 16b	39012	ELINT	CAST	198 sec
Yaogan 17c	39241	ELINT	SAST	165 sec
Yaogan 32a	43642	EO	CAST	75 sec

4.1 Yaogan 16b

The Yaogan 16b track showed the most dynamic behavior. Its lightcurve varied considerably over the 3 minutes of track, though the signature was not periodic. This does highlight a particular challenge in working with LEO satellites as the rapidly changing position relative to the sensor as well as the solar phase angle can exhibit very dynamic behavior which will be challenging to interpret. That being said, much more data will need to be collected to understand whether, in time, characteristics can be defined to be able to categorize in- and out-of-family signatures.

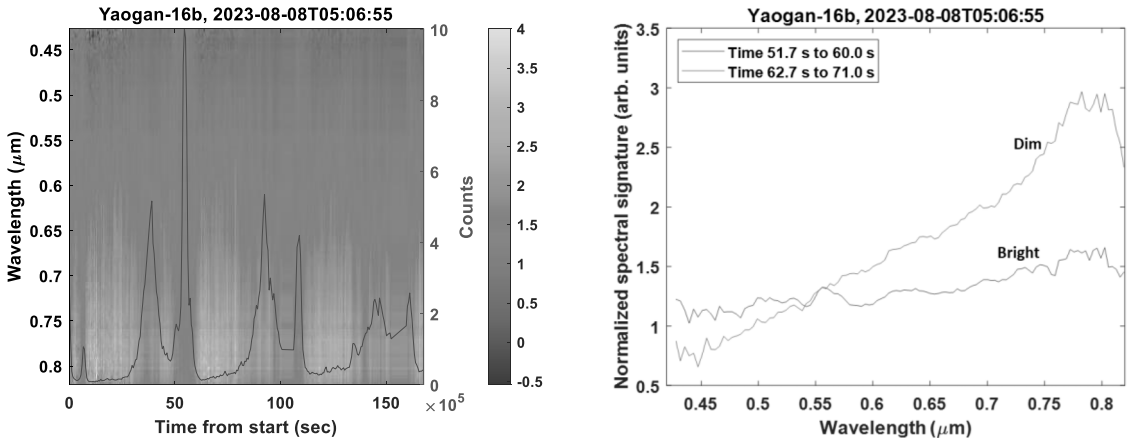

Figure 8: *Spectra results for Yaogan 16b. The left plot shows an overview of the waterfall plot of the spectra as a function of time, with the uncalibrated light curve (counts) overlaid. The colorbar refers to the color in the waterfall. On the right are spectra from different time windows, median filtered over that window. The plots correspond to times when the light curve was low (dim) and high (bright).*

The left figure shows a waterfall plot of the spectra versus time. The left figure also shows the uncalibrated light curve against the right y-axis overlaid on the waterfall spectra. The right plot shows selected bands (in time) of spectra which were median filtered in time to clean up the measurements. What is particularly interesting is that it appears that when the satellite is dimmer, it is usually redder (see the red trace in Fig. 8 right, from 62.7 to 71.0 seconds), whereas when the brightness increases, the spectra flattens (see the blue trace in Fig. 8 right, from 51.7 to 60.0 seconds). One could speculate that the brightness increases are due to something metallic and thus neutral in color glinting, such as antennae, etc.

4.2 Yaogan 17c

Yaogan 17c is in the same functional family as the 16 series, however the contractor who manufactured it is different. Its spectral signature waterfall plot and selected spectra are shown in Fig. 9.

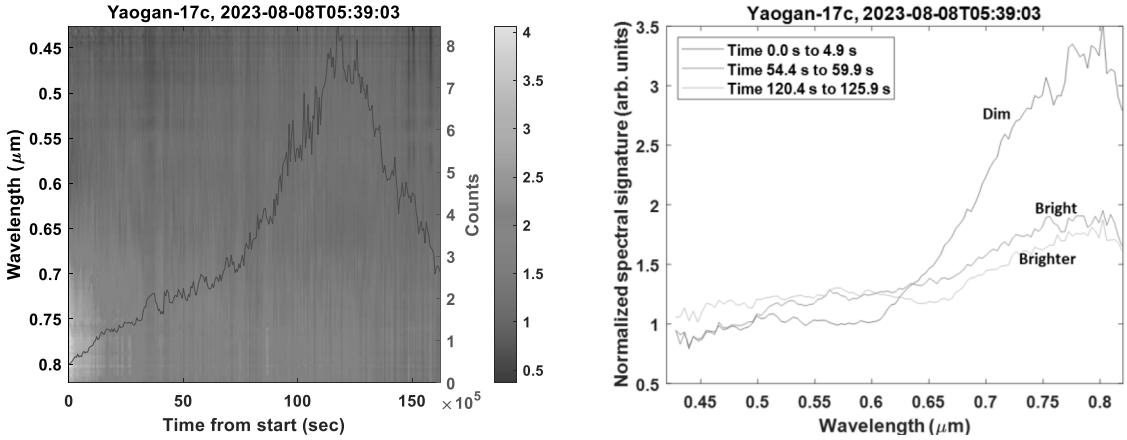

Figure 9: *Spectra results for Yaogan 17c. As in Fig. 9, waterfall spectra as a function of time is shown on the left, overlain with the uncalibrated light curve in counts. The colorbar maps to the spectral waterfall. On the right, selected time blocks of spectral data, median filtered.*

In this case, it's easily seen that the light curve is much more well behaved, though, again, there is some phenomenology which is making the spectra flatten out when it gets bright, while definitely being much more red when dim. There are clearly differences, however, between the 17c and the 16b. For one, the dim spectra on 16b (red trace in Fig. 8 on the right) shows a more gradual increase as a function of wavelength, while the 17c dim spectra (blue trace in Fig. 9 on the right) shows a sharp increase around 0.6 um.

4.3 Yaogan 32a

Yaogan 32a is of a different function than 16b or 17c, being an EO as opposed to ELINT satellite. Its waterfall spectra, light curve, and selected spectra are shown in Fig. 10.

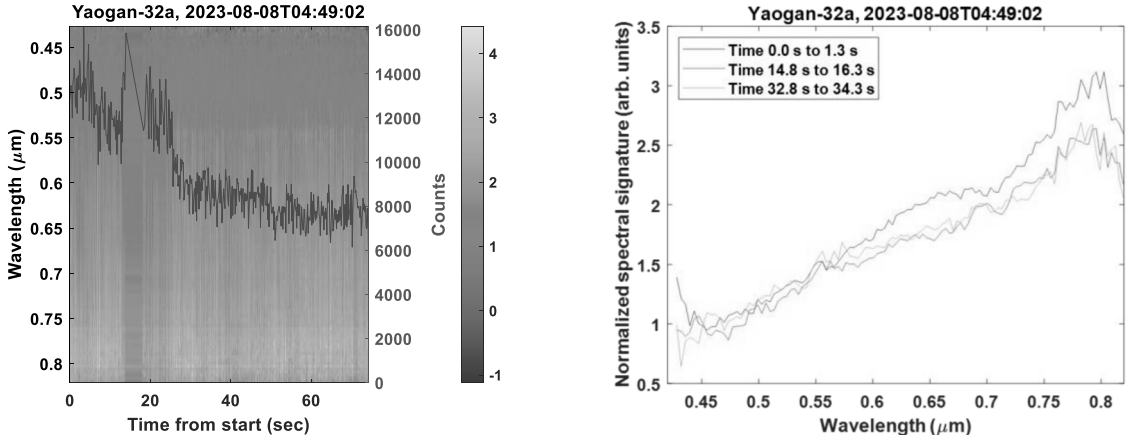

Figure 10: *Spectra results for Yaogan32a, the format the same as in Fig. 8 and 9. Of note is a block of time around 15-20 seconds – there was a loss of track in the data processing, so there is no data represented there.*

The results here show a much more stable spectra/light curve. Considering it is an EO satellite, and it was imaged at night, it's not unreasonable to assume that, since it probably was not doing mission (i.e., no slewing and pointing), its spectra would be more stable. Its spectra does show a similar characteristic to the dim states of 16b and 17c, in that it's definitely more red. Another point to make is that it's more like 16b since it does not show the upward bend in the spectral curve as seen in the dim 17c spectra. This could be an effect since 16b and 32a were both built by CAST, and 17c by SAST. Different contractors may use, for example, different types/brands of multi-layer insulation (MLI) which wraps the satellite to maintain thermal conditions, and in the dim states, the MLI may be the dominant component of its signature.

5. CONCLUSIONS AND PATH FORWARD

A simple modification to an existing tracking system, adding a transmission grating at the telescope exit pupil location prior to the imaging lens, was done to prototype a sensor for SDA which provides simultaneous track and spectral data on tracked satellites. The sensor system was made functional and preliminary testing was carried out. Due to the lateness of getting the sensor online, very little data was able to be collected, however what data was collected did begin to reveal some features of interest, as well as raise questions to be investigated.

- LEO satellites, by the nature of their dynamic relationship to the sensor and the sun's location, will always be more difficult to assess.
- When LEO light curves get bright, in this very small sample, they have tended to flatten out spectrally
- When LEO light curves are dimmer, they tend to go more reddish
- There are differences in dim signatures which may be attributable to manufacturer
- There might be a difference with the bright signatures as a function of manufacturer as well, but that is much more of a stretch.

The obvious caveat to any of these statements is that 3 tracks is a woefully inadequate sample to make any definitive statements regarding satellite characterization and identification.

Moving forward, with the sensor testbed fully functional, and the processing tools developed, the goal for the rest of the year's IRAD is to collect as much Yaogan satellite data as possible and begin assessing the similarities and differences manually. This is clearly a task that, once a larger data set is available, would be ideal for certain machine learning algorithms to work on. However, at this time, the data is so sparse, visual inspection is all that is planned for this year's IRAD.

If this task continues into 2024, there are some instrumental refinements and optimizations which could be made. The pixel-wavelength mapping is of some concern due to lack of range of Kr lines seen. The G2V calibration star data did not behave as expected, which is puzzling and needs to be understood. There are some issues with how the tracking was done in the telescope control system which caused some of the data to be unusable – these issues will be addressed.

6. REFERENCES

[1] A Speicher, et al., Results from an experiment that collected visible-light polarization data using unresolved imagery for classification of geosynchronous satellites, *SPIE Proceedings 946006* , 2015.
[2] P. Seitzer et. al., Visible Light Spectroscopy of GEO Debris, *AMOS Conference Proceedings*, 2012.
[3] D. Nishimoto et. al., " Spectroscopic observations of space objects and phenomena using Spica and Kala at AMOS," *SPIE Proceedings 4490*, San Diego CA, 2001.
[4] Schildknecht, T., et al., Reflectance Spectra of Space Debris in GEO, *AMOS Conference Proceedings*, 2009.
[5] Private conversation with Dave Monet, Small Telescope Workshop, 2019
[6] https://en.wikipedia.org/wiki/Yaogan
[7] R Shivitz, et al., Space Object Tracking (SPOT) facilty, *SPIE Proceedings 9145*, 91450J (2014).
[8] https://www.physics.nist.gov/PhysRefData/Handbook/Tables/kryptontable2.htm
[9] https://www.astromatic.net/software/sextractor/

7. TRANSFER OF COPYRIGHT

A signed statement of Transfer of Copyright must accompany your paper at time of submission in to be included in the Proceedings in which your paper will be published. The intent of this agreement is to protect the interests of both MEDB and authors/employers, and to specify reasonable rights for both parties related to publication and reuse of the material. Complete details of the agreement are presented on the form.